Physics of Plasmas

Electron acceleration based on Bloch surface waves

Cite as: Phys. Plasmas **29**, 063105 (2022); https://doi.org/10.1063/5.0086425
Submitted: 25 January 2022 • Accepted: 10 April 2022 • Published Online: 02 June 2022

Ying Bin Zhu, Pan Zhao, Mei Yan Liao, et al.

Physics of Plasmas ARTICLE scitation.org/journal/php

Electron acceleration based on Bloch surface waves

Cite as: Phys. Plasmas **29**, 063105 (2022); doi: 10.1063/5.0086425
Submitted: 25 January 2022 · Accepted: 10 April 2022 ·
Published Online: 2 June 2022

Ying Bin Zhu,[1,2,a)] Pan Zhao,[1,2] Mei Yan Liao,[1,2] Ruo He Yao,[1,2,b)] and L. K. Ang[3,c)]

AFFILIATIONS

[1]School of Electronic and Information Engineering, South China University of Technology (SCUT), Guangzhou 510006, China
[2]School of Microelectronics, South China University of Technology (SCUT), Guangzhou 510006, China
[3]Science, Mathematics and Technology Cluster, Singapore University of Technology and Design (SUTD), 8 Somapah Road, Singapore 487372, Singapore

[a)]Author to whom correspondence should be addressed: zhuyingbin@scut.edu.cn
[b)]phrhyao@scut.edu.cn
[c)]ricky_ang@sutd.edu.sg

ABSTRACT

In this paper, we present an electron acceleration model based on Bloch surface waves (BSWs). In our model, a dielectric multilayer deposited on a prism substrate is used to generate BSWs by a femtosecond laser pulse. It is found that the field enhancement factor of BSWs is larger than that of surface plasmon polaritons. We numerically solve Maxwell's equations to explain the phenomenon in space and time domain. Various aspects of the acceleration mechanism are discussed, including BSWs coupling and evanescent attenuation, the influence of electron injection time and angle, the kinetic energy spectrum, the angular distribution, and the angular-resolved energy spectrum. Such a model provides an all-optical method for electron acceleration.

I. INTRODUCTION

The acceleration of electrons has attracted much attention from researchers owing to their wide range of applications including high energy physics, x-ray light sources, and medical devices.[1–4] Electron acceleration devices based upon conventional radio-frequency (RF) technology are often large and expensive due to the accelerator length and total stored energy needed to accelerate electrons to high energy.[5,6] However, many applications require electron acceleration devices to reduce size and cost. To address these issues, many advanced electron acceleration devices have been proposed, including laser plasma acceleration (LPA), THz acceleration, and dielectric laser acceleration (DLA). LPA was originally proposed by Tajima and Dawson in 1979.[7] After that, several LPA devices have been proposed, including laser wakefield accelerator (LPWA),[8,9] accelerator based on surface plasmon polaritons (SPPs),[10–13] and plasma beat wave accelerator (PBWA).[14] THz acceleration is driven using single-cycle or multi-cycle terahertz pulses. THz accelerators are larger than LPAs and DLAs, so they are often used in intermediate-scale devices.[15,16] As we all know, the damage threshold of dielectrics is higher than that of metals, and all-dielectric structures are easy to fabricate with high quality at scale.[17,18] DLA is expected to be the main direction for the development of new accelerators.[18] However, all DLA devices were in the theoretical research stage[19–25] until two pioneering papers published by Peralta *et al.* in *Nature* and Breuer and Hommelhoff in *Phys. Rev. Lett.* started the experimental research on DLAs in 2013.[26,27] Since then, many related studies have been promoting the development of this field.[28–30] It was reported that on-chip acceleration provides the possibility for a completely integrated mega-electron volt-scale DLA.[28,29]

Bloch surface waves (BSWs) are evanescent electromagnetic surface waves excited at the interface between the truncated periodic dielectric multilayer film and vacuum, which have local enhancement properties and exhibit exponential decay in the perpendicular direction.[31] Compared with SPPs, BSWs have the advantages of lower loss and all-dielectric structure.[32] Therefore, BSWs have attracted much attention in the sensing field.[32–36] In particular, one of the fascinating characteristics of BSWs or SPPs is that their electromagnetic field can be greatly enhanced, which brings about the possibility of realizing an efficient electron acceleration with BSWs or SPPs. However, electron acceleration based on SPPs has been widely studied,[10,13,37,38] but there are few related studies about the electron acceleration by BSWs.[19]

In this paper, we report a new approach of using BSWs to accelerate electrons, which has a certain promotion effect on the study of

electron acceleration, especially the development of DLAs. There are two important steps to accelerate electrons using this approach. The first step is to excite the BSWs at the interface of the periodic dielectric multilayer film and vacuum via femtosecond laser pulses. The second key step is to inject electrons into the Bloch surface waves region at appropriate spatial and temporal scales and to calculate the electrons motion. In our model, we will study the scaling relation between the maximum kinetic energy and the incident angle of electrons, and the delay time between the electron pulse and BSWs under different condition. Simulation results show that final kinetic energy of electrons can be accelerated to a few keV or even tens of keV in the range of around 1 μm. Our results show that BSWs-based electron acceleration is superior to SPPs-based electron acceleration. Finally, the kinetic energy of accelerated electrons can be maximized by optimization of the operating parameters.

II. BSWs-BASED ELECTRON ACCELERATION MODEL

A basic schematic for generating BSWs to accelerate electrons is illustrated in Fig. 1. A femtosecond laser pulse with duration τ_p is incident on the truncated periodic multilayer dielectric film deposited on the prism substrate at the incident angle β. Since the wave vector of BSWs is larger than that of light in free space, wave vector compensation is required to excite BSWs. As shown in Fig. 1, this paper uses the commonly used Kretschmann–Raether structure to solve this problem. BSWs can be excited by regulating the incident angle β to satisfy the wave vector matching formula as[39]

$$K_{BSWs} = \frac{\omega}{c}\sqrt{\varepsilon_p}\sin\beta, \tag{1}$$

where ε_p is the dielectric constant of the prism, ω is the laser frequency, c is the speed of light, and K_{BSWs} is the wave vector of BSWs.

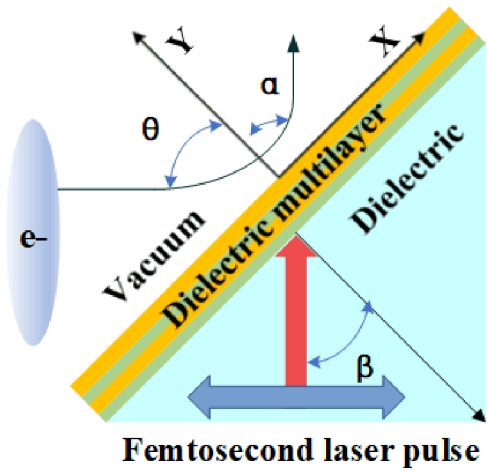

FIG. 1. The basic arrangement for electron accelerating using BSWs. BSWs are excited on the surface of the structure by a p-polarized femtosecond laser pulse at the incident angle β. An external electron beam is incident on the surface of the prism deposited with the dielectric multilayer at an angle θ, determined by the surface normal and incident direction. The electrons of the incident beam are deflected due to BSWs and leave the interaction region at an angle α, determined by the surface normal and departure direction.

When BSWs are excited, the electromagnetic (EM) field energy is converted into BSWs. The electric field distribution is given by

$$E_{BSWs}(y,t) = \eta E_l(t)\exp(-\gamma y), \tag{2}$$

where η is the electric field enhancement factor, $E_l(t)$ is the electric field envelope of the femtosecond laser pulse, γ^{-1} is the evanescent decay length into the vacuum, and y is the normal distance from the surface of the truncated periodic multilayer dielectric film. When the injected electrons with incident angle θ from the vacuum encounter the generated BSWs, their original linear motion pattern will be modified due to the action of BSWs. The direction of the ponderomotive force is along the largest field gradient, which is approximately normal to the surface of the dielectric multilayer. When an incident electron with energy less than the ponderomotive potential, it will be deflected and move away from the surface at an angle α.

In a practical setting, there is more than one injected electron. Electrons injected at different times or different locations will enter the BSWs region at different times and locations. Thus, only a portion of the electrons that have entered the BSWs region will gain enough momentum to redirect and move away from the surface of the dielectric multilayer, while others will collide with the surface. These electrons are considered to be completely absorbed by the dielectric multilayer and can be ignored. In our model, it will be demonstrated that the final kinetic energy and direction of an injected electron can be determined by θ, its injection time (a delay time relative to the excitation time of BSWs), and the parameters of the femtosecond laser pulse.

In the inset of Fig. 2, the structure of the truncated periodic dielectric multilayer film is illustrated. The refractive index of the glass (bottom layer) is 1.515. The structure is an 18-layer structure consisting of alternating cycles of Si_3N_4 and SiO_2. The SiO_2 layer has a low refractive index of $n = 1.48 + i10^{(-3)}$, while the Si_3N_4 layer has a refractive index of $n = 2.65 + i5 \times 10^{(-3)}$. Approximate periodic thicknesses are first determined by the quarter-wavelength formulation[40]

$$d_1 = \frac{\lambda}{4n_1\cos(\theta_1)}, \quad d_2 = \frac{\lambda}{4n_2\cos(\theta_2)}, \tag{3}$$

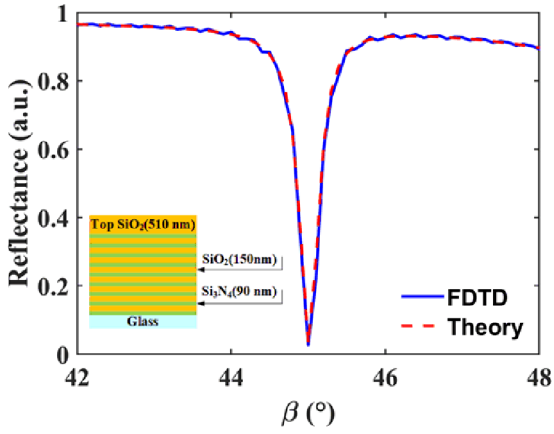

FIG. 2. The reflectance vs the incident angle β of a p-polarized femtosecond laser pulse with a wavelength of 800 nm. The inset shows the structure of the truncated periodic dielectric multilayer film.

where n_1/d_1 and n_2/d_2 are refractive index/thicknesses of Si_3N_4 and SiO_2, respectively; θ_1 and θ_2 are incident angle inside Si_3N_4 and SiO_2 layers, respectively; and λ is an operating wavelength. The thickness of the top layer is obtained through multiple simulation comparisons and optimizes them further. In this paper, the thicknesses of SiO_2 and Si_3N_4 layers are 150 and 90 nm, respectively. The thickness of the top SiO_2 layer is 510 nm. Obtaining the time and space distribution of the electromagnetic field above the surface of the structure is necessary to calculate the electron motion near dielectric surface. We solve Maxwell's equations given by

$$\frac{d\mathbf{H}}{dt} = -\frac{1}{\mu_0}\nabla \times \mathbf{E} \tag{4}$$

and

$$\frac{d\mathbf{E}}{dt} = \frac{1}{\varepsilon}\nabla \times \mathbf{H}, \tag{5}$$

where $\mathbf{H}$ is the magnetic field, $\mathbf{E}$ is the electric field, ε is the local permittivity, and μ_0 is the permeability of free space. The exact analytical solutions for these equations is hard for the given structure, so we numerically solve Eqs. (4) and (5) using a two-dimensional finite-difference time-domain technique (FDTD).[41] In our model, the electromagnetic wave is excited via a femtosecond laser, and a perfectly matched layer is used to attenuate false reflections from the window boundaries. The motion of injected electrons in the numerically solved electromagnetic field is governed by the Lorentz equation as

$$\frac{d\mathbf{v}}{dt} = \frac{q}{m}(\mathbf{E} + \mu_0 \mathbf{v} \times \mathbf{H}), \tag{6}$$

where v and q/m are the velocity and charge-to-mass ratio of the electron, respectively. In our model, the incident electron beam consists of approximately 10^5 test electrons, which are assigned the same weight within the limited spatial and temporal extent of the packet. Since we do not consider space charge effects, we must ensure that the current density is lower than the space charge current density 10^4 A/cm^2, below which the Coulomb force between the injected electrons is negligible compared to the force of the BSWs on the electrons.[42] If the current density exceeds 10^4 A/cm^2, the space charge algorithm can be added to our calculation process.[43,44] In addition, for simplicity, the secondary electron emission is not considered here, which means that any electrons reaching the surface of the dielectric multilayer film are assumed to be absorbed.

Figure 2 shows the relationship of reflectivity vs the incident angle β, where the blue solid line and the red dashed line represent the FDTD-based results and theoretical calculation results using the transfer matrix method,[45] respectively. The two curves are in nice agreement, and it shows a narrow and sharp dip at the angle of $\beta = 45°$, which is the best matching angle to excite BSWs.

In this paper, we used the FDTD method to numerically calculate the electromagnetic field distribution in the structure. The femtosecond laser has a wavelength of $\lambda = 800$ nm, a pulse width of $\tau_p = 20$ fs, and an incident angle of $\beta = 45°$. Sufficiently small mesh size of the computational lattice is chosen to be $\Delta x, \Delta y = 0.25$ nm. The corresponding temporal step size of $\Delta t = 9 \times 10^{-3}$ fs is used in the calculation.

III. RESULTS AND ANALYSIS

The local spatial and temporal distribution of the electromagnetic field of BSWs is important to our research. Figure 3(a) depicts the normalized electric field intensity distribution of BSW in TM mode, which has a peak at the interface ($y = 0$) of the vacuum and the dielectric multilayers film, and then decreases exponentially in the vacuum region ($y > 0$) away from the interface. Figure 3(b) shows the corresponding normalized magnetic field intensity distribution of BSWs in TM mode, which has the same profile in the vacuum region as the electric field in TM-BSWs modes. However, the magnetic field has two peaks, both of which are inside the top layer SiO_2.

Figure 4 illustrates the fitting analysis results of the electric field intensity distribution of TM-BSWs in the vacuum region. The results indicate that the electric field enhancement factor and vacuum decay length of TM-BSWs are $\eta = 8.8508$ and $\alpha^{-1} = 333$ nm, respectively. Here, we only fit and analyze the electric field. Since the force of the magnetic field on the electrons is much smaller than that of the electric field (during our calculations, the ratio of the magnetic field force to the electric field force is about 10^{-2}), its effect can be ignored. This can simplify the computational complexity. It is important to note that enhancement factors of SPPs of the one-pulse excitation scheme reported in Refs. 12 and 13 are 3.7 and 4.675, respectively. Therefore, using the same femtosecond laser pulse, the field strength of BSWs is about twice that of SPPs. In addition, the attenuation length of SPPs in the vacuum is $\alpha^{-1} = 250$ nm,[10–13] which is shorter than that of BSWs. These comparison results show that under the same conditions, BSWs provide a stronger field and a larger range of action for electron acceleration compared with SPPs, so it can be predicted that electrons will gain greater energy for BSWs-based electron acceleration. The E_x/E_y

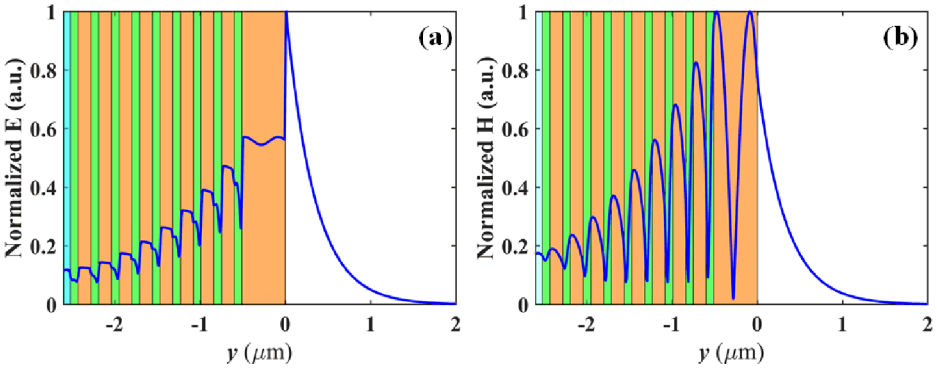

FIG. 3. Field distribution for TM-BSWs modes along the y direction. (a) Normalized electric field strength distribution. (b) Normalized magnetic field strength distribution. $y = 0$ nm represents the spatial position of the upper surface of the top SiO_2.

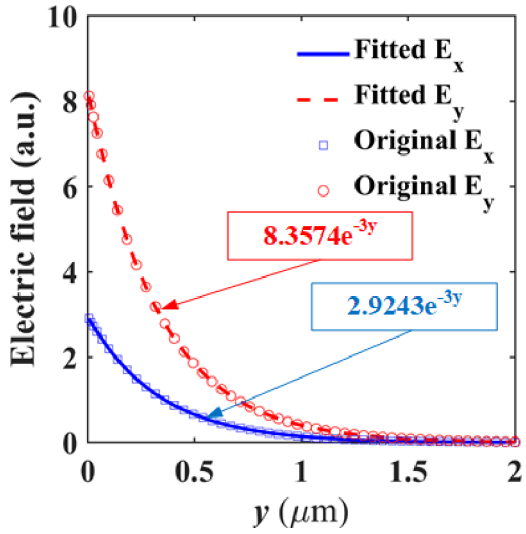

FIG. 4. Fitting analysis of electric field in TM-BSWs mode. Square and round marks represent the original data obtained by the FDTD method, while solid and dashed lines describe the fitting results on the original data.

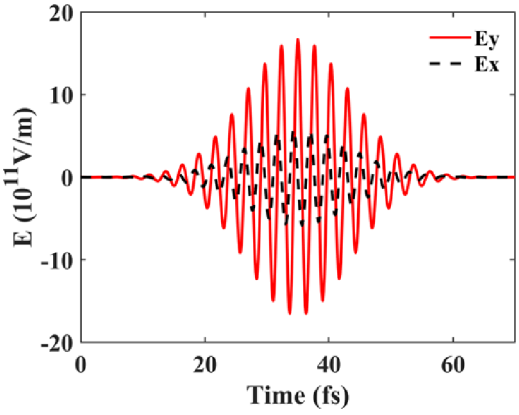

FIG. 5. Time-dependent electric field of TM-BSWs on the upper surface central of the top SiO_2 layer.

ratio of BSWs field is 0.3499, which is smaller than the value 0.45 of SPPs field.[13] This indicates that the movement of the electrons is mainly controlled by E_y, which will be reflected in the electron trajectory diagram in Fig. 6(a). The above results are consistent with the physical properties of BSWs. Figure 5 shows the time profile of the electric field in TM-BSWs on the upper surface center of the top SiO_2 layer, while the femtosecond laser pulse intensity is set as $E_l = 10^{11}$ V/m.[11] Clearly, the electric field envelope is similar to that of the femtosecond laser pulse, but with a wider duration. This is because the field strength increases, but the trend of the field strength over time does not change. In addition, Fig. 5 indicates that the E_y is delayed a phase $\pi/2$ with respect to E_x.

To illustrate the motion of electrons in BSWs, five test electrons were injected to study their trajectories, which are shown in the Fig. 6(a). The test electrons are injected with incident angle $\theta = 45°$ and initial kinetic energy $E_{k0} = 1$ keV. Their delay times are $\tau_e = -30$, -27, -24, -21, and -18 fs, respectively. Here, 0 fs corresponds to the time when the femtosecond laser pulse excites the BSWs. In addition, their corresponding outgoing energy is as follows: 5.8, 4.7, 3.7, 2.8, and 2.2 keV, respectively. This indicates that electrons can be accelerated to a few keV at ~ 1 μm. Their trajectories simply describe the effect of BSWs on the motion process of the injected electrons. When electrons enter the field of BSWs, their inherently linear and uniform motion will be significantly influence by BSWs. This is clearly evidenced by the "quivering" in their trajectories. Furthermore, their trajectories also suggest that electrons injected with different delay times will have different exit angles. It can be seen from Fig. 6(a) that the exit angle of the injected electron with a delay time of -18 fs (green solid line) is larger than that of the injected electron with a delay time of -30 fs (blue solid line). This is determined by the properties of BSWs. Electrons closer to the surface will experience stronger BSWs fields. As shown in Fig. 6(a), their deflection positions gradually move away from the surface as the absolute value of the delay time decreases. In addition, the electric field is stronger in the y direction than in the x direction, so the larger the absolute value of the delay time, the smaller their exit angle. However, it should be noted that electrons with too large absolute delay time will hit the surface directly.

Figure 6(b) clearly shows the exit angle of the electron and its final kinetic energy vs the delay time. Interestingly, the exit angle α and the delay time are roughly positively correlated (red solid line), while the final kinetic energy and delay time are roughly negatively

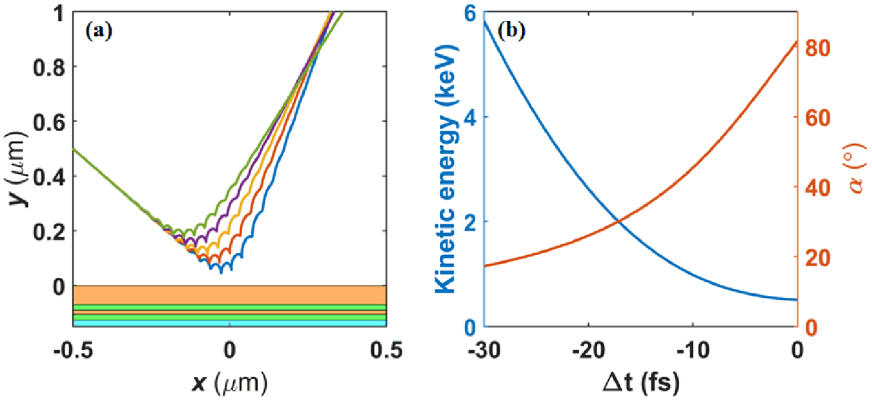

FIG. 6. (a). Trajectories of five test electrons as they move in the field of the TM-BSWs excited by a femtosecond laser with a peak electric field amplitude of $E_l = 10^{11}$ V/m. The injection times of the test electrons (the delay time relative to the excitation time of the TM-BSWs) are $\tau_e = -30$ (blue), -27 (red), -24 (orange), -21 (purple), and -18 fs (green), respectively. (b). The solid blue line represents the relationship between the final kinetic energy of the electron and its delay time. The solid red line represents the relationship between the final electron exit angle and its delay time. Here, we assume that an electron beam containing $\sim 10^3$ electrons is injected discretely from the same location over a period of time.

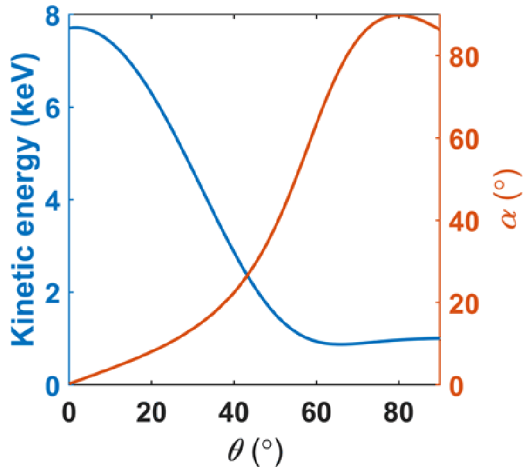

FIG. 7. The solid blue line represents the relationship between the final kinetic energy of the outgoing electrons and its angle of incidence. The red solid line represents the relationship between the exit angle of the outgoing electrons and its incident angle. Here, we assume that electrons are injected from the same location at the same delay time −18 fs at different angles of incidence.

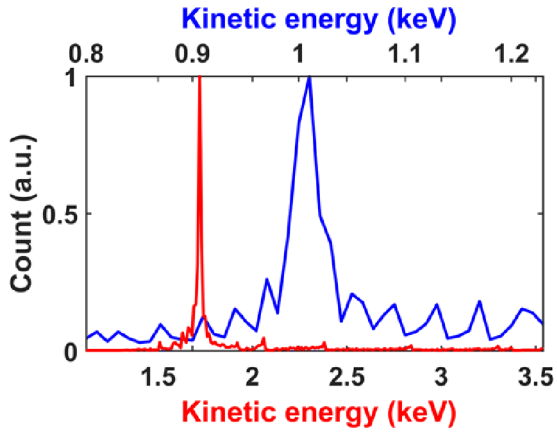

FIG. 9. The energy spectrum of the accelerated electrons of $E_l = 10^{10}$ V/m (blue line, top) and $E_l = 4 \times 10^{10}$ V/m (red line, bottom). It is assumed that $\sim 10^3$ electrons uniformly distributed over a certain time range are incident at nearly 90° from the same location with an initial kinetic energy of 1 keV.

correlated (blue solid line). This indicates that electrons that have a chance to approach the surface without colliding will have a greater final kinetic energy. In addition, when the delay time is close to 0 fs, the final kinetic energy of the outgoing electrons converges asymptotically to around 510 eV, and its exit angle asymptotically converges to around 90°. This means that the V_y of some electrons decreases close to 0, while their V_x is basically unchanged. This further suggests that the motion of the electrons in the x direction contributes less to the final kinetic energy of the outgoing electrons.

Figure 7 clearly shows the exit angle of the electron and its final kinetic energy vs the incident angle θ. As the incident angle is increasing, the final kinetic energy of the outgoing electron decrease and the exit angle increase. Particularly, as the incident angle θ approaches 90°, the energy gradually converges to a value close to 1 keV. This indicates that BSWs have little effect on electrons injected parallel to the surface at a certain height (determined by the decay length of BSWs) from the surface due to the exponential decay property of BSWs. However, those injected electrons directed toward the surface can be accelerated by BSWs more efficiently, as long as the delay time is appropriate.

Both Figs. 6 and 7 indicate a conclusion that electrons moving near the surface of the structure without hitting the surface can be accelerated more efficiently by the BSWs. We have verified it with laser field strengths of 0.4×10^{10} V/m,[13] 1.5×10^{11} V/m, 2×10^{11} V/m, etc.

The kinetic energy spectrum of the outgoing electrons is shown in Fig. 8(a). Here, it is observed that a peak occurring at 510 eV, which indicates that portions of the electrons lose energy during the deflection process. According to statistics, the energy of 17.62% of the electrons is less than 1 keV. This shows that the energy of most electrons increases during the acceleration of BSWs. In addition, 22.19% of the emitted electrons have an energy greater than 5 keV and a small number of electrons even have an energy close to 8 keV. The angular distribution in the inset of Fig. 8(a) shows that the outgoing electrons have a highly directional property. Interestingly, there are significant number of electrons emitting at 90°, which indicates that some electrons are slowed down to a critical value where V_y is 0. This is shown more clearly in the angle-resolved spectrum of the outgoing electrons in Fig. 8(b). In addition, Fig. 8(b) clearly illustrates that the final energy of the outgoing electrons has a strong correlation with its outgoing angle. As the exit angle α approaches 90°, the energy of emergent electrons asymptotically converges to a value near 510 eV. When the other relevant parameters remain unchanged, the final kinetic energy of

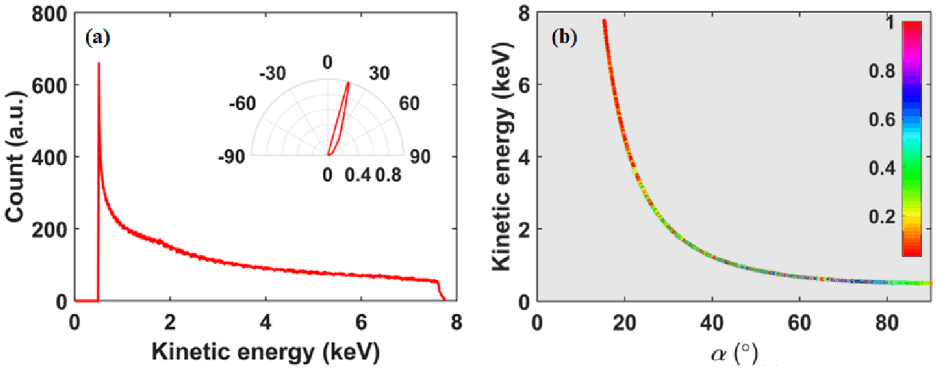

FIG. 8. (a) The kinetic energy spectra of the accelerated electrons. The inset shows the angular distribution of the accelerated electrons, which has a peak at 15.7° and an angular half-width of 8.5°. (b) The angular resolved kinetic energy spectrum. The color bar represents the relative number of outgoing electrons at that point. The closer the color is to 1, the higher the number of electrons. Here, it is assumed that $\sim 10^5$ electrons are injected discretely from a finite spatial and temporal scale with delay times ranging from −30 to −10 fs, and an incident angle of 45°.

accelerated electron can reach 20 and 25 keV when using a femtosecond laser with $E_l = 2 \times 10^{11}$ V/m and $E_l = 2.5 \times 10^{11}$ V/m, respectively. This suggests that by increasing the intensity of the femtosecond laser, the outgoing electrons also can gain greater final kinetic energy. Furthermore, as shown in Fig. 9, when the peak electric field of the laser pulse is $E_l = 10^{10}$ V/m, the maximum energy of the outgoing electrons can reach 1.24 keV; when the peak electric field is $E_l = 4 \times 10^{10}$ V/m, the maximum energy of the outgoing electrons can reach 3.54 keV. This indicates that a good acceleration effect can also be obtained when the conditions are suitable and the laser intensity is reduced.

IV. CONCLUSIONS

This paper has theoretically proposed a novel scheme for electron acceleration using BSWs. We study the properties of BSWs and the acceleration process of electrons in BSWs. In addition, the effect of some variables, including electron incident angle and electron injection time on the electron exit results, is studied. It is concluded that the electron exit kinetic energy can be increased by reasonably adjusting the electron incident angle and incident time. Furthermore, it is found that under certain conditions, the initial kinetic energy of injected electrons can be enhanced several or even dozens of times when amplitude of the femtosecond laser pulses is large enough. Such a model provides an all-optical method for electron acceleration.

ACKNOWLEDGMENTS

This work was supported in part by the National Natural Science Foundation of China (No. 61801182), State Key Laboratory of Optoelectronic Materials and Technologies Open Fund, Sun Yat-Sen University (No. OEMT-2018-KF-07), and Start-up Funding of School of Microelectronics, South China University of Technology (SCUT) (No. K5200280).

AUTHOR DECLARATIONS

Conflict of Interest

The authors have no conflicts to disclose.

DATA AVAILABILITY

The data that support the findings of this study are available from the corresponding author upon reasonable request.

REFERENCES

[1]L. Robson, P. T. Simpson, R. J. Clarke, K. W. D. Ledingham, F. Lindau, O. Lundh, T. McCanny, P. Mora, D. Neely, C.-G. Wahlström, M. Zepf, and P. McKenna, Nat. Phys. **3**, 58 (2007).
[2]H. B. Zhuo, Z. L. Chen, W. Yu, Z. M. Sheng, M. Y. Yu, Z. Jin, and R. Kodama, Phys. Rev. Lett. **105**, 065003 (2010).
[3]A. H. Zewail, Science **328**, 187 (2010).
[4]M. Gulde, S. Schweda, G. Storeck, M. Maiti, H. K. Yu, A. M. Wodtke, S. Schäfer, and C. Ropers, Science **345**, 200 (2014).
[5]X. Y. Lu, J. F. Picard, M. A. Shapiro, I. Mastovsky, R. J. Temkin, M. Conde, J. G. Power, J. H. Shao, E. E. Wisniewski, M. M. Peng, G. Ha, J. Seok, S. Doran, and C. G. Jing, Appl. Phys. Lett. **116**, 264102 (2020).
[6]A. Nassiri, B. Chase, P. Craievich, A. Fabris, H. Frischholz, J. Jacob, E. Jensen, M. Jensen, R. Kustom, and R. Pasquinelli, IEEE Trans. Nucl. Sci. **63**, 707 (2016).
[7]T. Tajima and J. M. Dawson, Phys. Rev. Lett. **43**, 267 (1979).
[8]E. Gschwendtner and P. Muggli, Nat. Rev. Phys. **1**, 246 (2019).
[9]E. Esarey, C. B. Schroeder, and W. P. Leemans, Rev. Mod. Phys. **81**, 1229 (2009).
[10]S. E. Irvine, A. Dechant, and A. Y. Elezzabi, Phys. Rev. Lett. **93**, 184801 (2004).
[11]S. E. Irvine and A. Y. Elezzabi, Phys. Rev. Appl. **73**, 013815 (2006).
[12]S. E. Irvine and A. Y. Elezzabi, Opt. Express **14**, 4115 (2006).
[13]P. F. Lu, J. Wu, H. X. Qi, and H. P. Zeng, Opt. Express **17**, 4367 (2009).
[14]M. N. Rosenbluth and C. S. Liu, Phys. Rev. Lett. **29**, 701 (1972).
[15]S. L. Lange, N. K. Noori, T. M. B. Kristensen, K. Steenberg, and P. U. Jepsen, J. App. Phys. **128**, 070901 (2020).
[16]E. A. Nanni, W. R. Huang, K. H. Hong, K. Ravi, A. Fallahi, G. Moriena, R. J. D. Miller, and F. X. Kärtner, Nat. Commun. **6**, 8486 (2015).
[17]M. Lenzner, J. Krüger, S. Sartania, Z. Cheng, Ch. Spielmann, G. Mourou, W. Kautek, and F. Krausz, Phys. Rev. Lett. **80**, 4076 (1998).
[18]R. J. England, R. J. Noble, K. Bane, D. H. Dowell, C. K. Ng, J. E. Spencer, S. Tantawi, and Z. R. Wu, Rev. Mod. Phys. **86**, 1337 (2014).
[19]A. Mizrahi and L. Schächter, Phys. Rev. E **70**, 016505 (2004).
[20]B. Naranjo, A. Valloni, S. Putterman, and J. B. Rosenzweig, Phys. Rev. Lett. **109**, 164803 (2012).
[21]T. Plettner, P. P. Lu, and R. L. Byer, Phys. Rev. Spec. Top.—Accel. Beams **9**, 111301 (2006).
[22]X. E. Lin, Phys. Rev. Spec. Top.—Accel. Beams **4**, 051301 (2001).
[23]F. Luan, A. K. George, T. D. Hedley, G. J. Pearce, D. M. Bird, J. C. Knight, and P. S. J. Russell, Opt. Lett. **29**, 2369 (2004).
[24]J. Broeng, S. E. Barkou, T. Søndergaard, and A. Bjarklev, Opt. Lett. **25**, 96 (2000).
[25]Z. R. Wu, R. J. England, C. K. Ng, B. Cowan, C. McGuinness, C. Lee, M. H. Qi, and S. Tantawi, Phys. Rev. Spec. Top.—Accel. Beams **17**, 081301 (2014).
[26]J. Breuer and P. Hommelhoff, Phys. Rev. Lett. **111**, 134803 (2013).
[27]E. A. Peralta, K. Soong, R. J. England, E. R. Colby, Z. Wu, B. Montazeri, C. McGuinness, J. McNeur, K. J. Leedle, D. Walz, E. B. Sozer, B. Cowan, B. Schwartz, G. Travish, and R. L. Byer, Nature **503**, 91 (2013).
[28]N. V. Sapra, K. Y. Yang, D. Vercruysse, K. J. Leedle1, D. S. Black, R. J. England, L. Su, R. Trivedi, Y. Miao, O. Solgaard, R. L. Byer, and J. Vuković, Science **367**, 79 (2020).
[29]R. Shiloh, J. Illmer, T. Chlouba, P. Yousefi, N. Schönenberger, U. Niedermayer, A. Mittelbach, and P. Hommelhoff, Nature **597**, 498 (2021).
[30]Y. Adiv, K. P. Wang, R. Dahan, P. Broaddus, Y. Miao, D. Black, K. Leedle, R. L. Byer, O. Solgaard, R. J. England, and I. Kaminer, Phys. Rev. X **11**, 041042 (2021).
[31]R. X. Wang, Y. Wang, D. G. Zhang, G. Y. Si, L. F. Zhu, L. P. Du, S. S. Kou, R. Badugu, M. Rosenfeld, J. Lin, P. Wang, H. Ming, X. C. Yuan, and J. R. Lakowicz, ACS Nano **11**, 5283 (2017).
[32]R. X. Wang, H. Y. Xia, D. G. Zhang, J. X. Chen, L. F. Zhu, Y. Wang, E. C. Yang, T. Y. Zang, X. L. Wen, G. Zou, P. Wang, H. Ming, R. Badugu, and J. R. Lakowicz, Nat. Commun. **8**, 14330 (2017).
[33]J. X. Chen, D. G. Zhang, P. Wang, H. Ming, and J. R. Lakowicz, Phys. Rev. Appl. **9**, 024008 (2008).
[34]Y. H. Li, T. L. Yang, S. M. Song, Z. Y. Pang, G. Q. Du, and S. H. Han, Appl. Phys. Lett.**103**, 041116 (2013).
[35]I. Degli-Eredi, J. E. Sipe, and N. Vermeulen, Opt. Lett. **43**, 1095 (2018).
[36]C. Genet and T. W. Ebbesen, Nature **445**, 39 (2007).
[37]L. B. Kong, C. P. Huang, C. H. Du, P. K. Liu, and X. G. Yin, Sci. Rep. **5**, 1 (2015).
[38]L. B. Kong and Z. Y. Chen, Phys. Plasmas **24**, 083111 (2017).
[39]M. Gerlinger, A. J. Rowan, S. Horswell, J. Larkin, D. Endesfelder, E. Gronroos, P. Martinez, N. Matthews, A. Stewart, P. Tarpey, I. Varela, B. Phillimore, S. Begum, N. Q. McDonald, A. Butler, D. Jones, K. Raine, C. Latimer, C. R. Santos, M. Nohadani, A. C. Eklund, B. Spencer-Dene, G. Clark, L. Pickering, G. Stamp, M. Gore, Z. Szallasi, J. Downward, P. A. Futreal, and C. Swanton, New. Engl. J. Med. **366**, 883 (2012).
[40]A. Yariv and P. Yeh, *Photonics: Optical Electronics in Modern Communications* (Oxford University Press, Oxford, 2007).
[41]A. Taflove and S. C. Hagness, *Computational Electrodynamics: The Finite-Difference Time-Domain Method*, 3rd ed. (Artech House, Boston, 2005).
[42]J. P. Girardeau-Montaut and C. Girardeau-Montaut, J. Appl. Phys. **65**, 2889 (1989).
[43]Y. B. Zhu and L. K. Ang, Appl. Phys. Lett. **98**, 051502 (2011).
[44]Y. B. Zhu, P. Zhang, A. Valfells, L. K. Ang, and Y. Y. Lau, Phys Rev. Lett. **110**, 265007 (2013).
[45]P. Yeh, A. Yariv, and C. Hong, J. Opt. Soc. Am. **67**, 423 (1977).